# Light-Induced Renormalization of the Dirac Quasiparticles in the Nodal-Line Semimetal ZrSiSe

G. Gatti,[1,2] A. Crepaldi,[1,2,*] M. Puppin,[2,3] N. Tancogne-Dejean,[4] L. Xian,[4] U. De Giovannini,[4] S. Roth,[1,2] S. Polishchuk,[2,3] Ph. Bugnon,[1] A. Magrez,[1] H. Berger,[1] F. Frassetto,[5] L. Poletto,[5] L. Moreschini,[6,7] S. Moser,[6,8] A. Bostwick,[6] Eli Rotenberg,[6] A. Rubio,[4,9,10] M. Chergui,[2,3] and M. Grioni[1,2]

[1]*Institute of Physics, Ecole Polytechnique Fédérale de Lausanne (EPFL), CH-1015 Lausanne, Switzerland*
[2]*Lausanne Centre for Ultrafast Science (LACUS), Ecole Polytechnique Fédérale de Lausanne (EPFL), CH-1015 Lausanne, Switzerland*
[3]*Laboratory of Ultrafast Spectroscopy, ISIC, Ecole Polytechnique Fédérale de Lausanne (EPFL), CH-1015 Lausanne, Switzerland*
[4]*Max Planck Institute for the Structure and Dynamics of Matter and Center for Free-Electron Laser Science, Luruper Chaussee 149, Hamburg 22761, Germany*
[5]*National Research Council-Institute for Photonics and Nanotechnologies (CNR-IFN), via Trasea 7, 35131 Padova, Italy*
[6]*Advanced Light Source, Lawrence Berkeley National Laboratory, Berkeley, California 94720, USA*
[7]*Department of Physics, University of California–Berkeley, Berkeley, California 94720, USA*
[8]*Physikalisches Institut and Würzburg-Dresden Cluster of Excellence ct.qmat, Universität Würzburg, Würzburg 97074, Germany*
[9]*Nano-Bio Spectroscopy Group, Departamento de Fisica de Materiales, Universidad del País Vasco, San Sebastian 20018, Spain*
[10]*Center for Computational Quantum Physics, Flatiron Institute, New York, New York 10010, USA*

(Received 13 December 2019; accepted 17 July 2020; published 12 August 2020)

In nodal-line semimetals, linearly dispersing states form Dirac loops in the reciprocal space with a high degree of electron-hole symmetry and a reduced density of states near the Fermi level. The result is reduced electronic screening and enhanced correlations between Dirac quasiparticles. Here we investigate the electronic structure of ZrSiSe, by combining time- and angle-resolved photoelectron spectroscopy with *ab initio* density functional theory (DFT) complemented by an extended Hubbard model (DFT + $U$ + $V$) and by time-dependent DFT + $U$ + $V$. We show that electronic correlations are reduced on an ultrashort timescale by optical excitation of high-energy electrons-hole pairs, which transiently screen the Coulomb interaction. Our findings demonstrate an all-optical method for engineering the band structure of a quantum material.

DOI: 10.1103/PhysRevLett.125.076401

The application of topological concepts to condensed matter, which is central to the description of the quantum spin Hall effect [1] and topological insulators [2], has been fruitful in the classification of gapless topological phases [3–5]. Dirac and Weyl fermions emerge as low energy excitations, characterized by a discrete number of symmetry-protected nodes [6]. The nodes are responsible for magneto-transport properties that are unknown in topologically trivial compounds [7]. The nodes also exhibit vanishing density of states, which alter the screening of the Coulomb interaction, thus requiring corrections to the Fermi liquid model. Logarithmic corrections play an important role in two-dimensional (2D) compensated semimetals such as graphite [8] and graphene [9]. In the case of Dirac and Weyl particles, the reduced screening enhances correlations, affects charge transport [10] and makes the system prone to instabilities towards new ordered phases [11–13].

The long-range Coulomb interaction has been theoretically discussed in nodal-line semimetals (NLSMs) [14], where the intersection of linearly dispersing states forms 1D trajectories in reciprocal space [4,15,16]. It has been shown that in the low-doping regime of NLSMs, even if the Dirac lines are moved away from the Fermi level, weak screening affects the transport properties [17]. Similarly to the Dirac and Weyl semimetals, correlations can drive the materials to symmetry-broken ground states in the bulk [11] and at the surface [15].

NLSMs are realized in several families of square-net materials [18]. Zr$XY$ ($X$ = Si, Sn, Ge; $Y$ = S, Se, Te) is among the most studied, owing to the great flexibility of the chemical composition, and the high crystal quality which enable to reach the quantum limit in transport at relatively low magnetic field. The appearance of oscillation in the magnetic response [19,20] and in the resistivity [21–23], and the Berry phases extracted from these experiments, bear fingerprints of the nontrivial topology [21]. Magneto-transport measurements under high magnetic field have revealed an enhancement of the effective mass, which is interpreted as a signature of electronic correlations [24]. A reduction of the Drude peak and a transfer of spectral weight over a large energy range has been reported by magneto optics, and this effect was ascribed to

 

short-range interactions [25]. These findings are supported by theoretical models predicting a large excitonic instability in both ZrSiS [26] and in ZrSiSe [27], as a consequence of the reduced screening, combined with a large degree of electron-hole symmetry and with a finite density of itinerant charge carriers [26].

Several angle-resolved photoelectron spectroscopy (ARPES) studies have addressed the band structure of ZrSiSe [28–32], but no experimental evidence of band renormalization has been reported so far. In this Letter, we show that electronic correlations in ZrSiSe can be modified at the ultrashort timescale by an optical perturbation. The intense laser pulse creates electrons and holes far from the Dirac nodes, which efficiently screen the Coulomb interaction, leading to a renormalization of the Dirac quasiparticles (QP) dispersion probed by time-resolved ARPES (TR-ARPES). This interpretation is supported by *ab initio* density functional theory (DFT) calculations complemented by an extended Hubbard model (DFT + $U$ + $V$) [33] and by time-dependent DFT + $U$ + $V$.

High quality single crystals of ZrSiSe grown by vapor transport were cleaved *in situ* under ultrahigh vacuum (UHV) conditions. We measured the band structure by ARPES at the MAESTRO beam line 7.0.2 of the Advanced Light Source (ALS) in Berkeley, with overall energy and momentum resolutions equal to 0.01 Å$^{-1}$ and 30 meV. We performed measurements at the TR-ARPES end station [34] of the Harmonium facility [35] at the EPFL. We used $s$-polarized light at 36.9 eV photon energy, corresponding to the 23rd harmonic generated in argon. The optical excitation was $s$ polarized and centered at 1.6 eV (780 nm), with an absorbed fluence of 0.38 mJ/cm$^2$ estimated using optical properties from Refs. [36,37]. The temporal overlap between pump and probe was determined by the observation of the laser assisted photoelectric effect for $p$-polarized optical excitation. All measurements were performed at 80 K.

The band structure calculations were performed on a fully relaxed slab composed of five layers of ZrSiSe. We evaluated the on site $U$ and intersite $V$ Coulomb terms *ab initio* and self-consistently using the recently developed extended ACBN0 functional [33] of the Octopus code [38]. The Hubbard $U$ was evaluated for the $d$ orbitals of Zr, and limited to the nearest-neighbor interaction for the intersite $V$. We employed fully relativistic pseudopotentials with a $15 \times 15$ **k**-point grid and a grid spacing of 0.158 Å$^{-1}$ to sample the two-dimensional Brillouin zone. More details about geometry optimization and a comparison with DFT + $U$ and hybrid functionals can be found in the Supplemental Material [39–51].

The band structure of ZrSiSe hosts two kinds of nodal lines; one is protected by the nonsymmorphic symmetry and is located far from the Fermi level, $E_F$, along the bulk $X - R$ direction [28,31]. The second, more relevant for the screening and the transport properties, is formed by the crossing of the conduction band (CB) and valence band (VB), as schematized in Fig. 1(a). Near $E_F$, the bulk bands are approximately linear, with a nonvanishing but small density of states. This combined with a large electron-hole symmetry is responsible for the relatively poor screening of the long-range Coulomb interaction. The goal of our study is to transiently enhance the screening by optically exciting high-energy electrons-hole pairs far from the Dirac nodes.

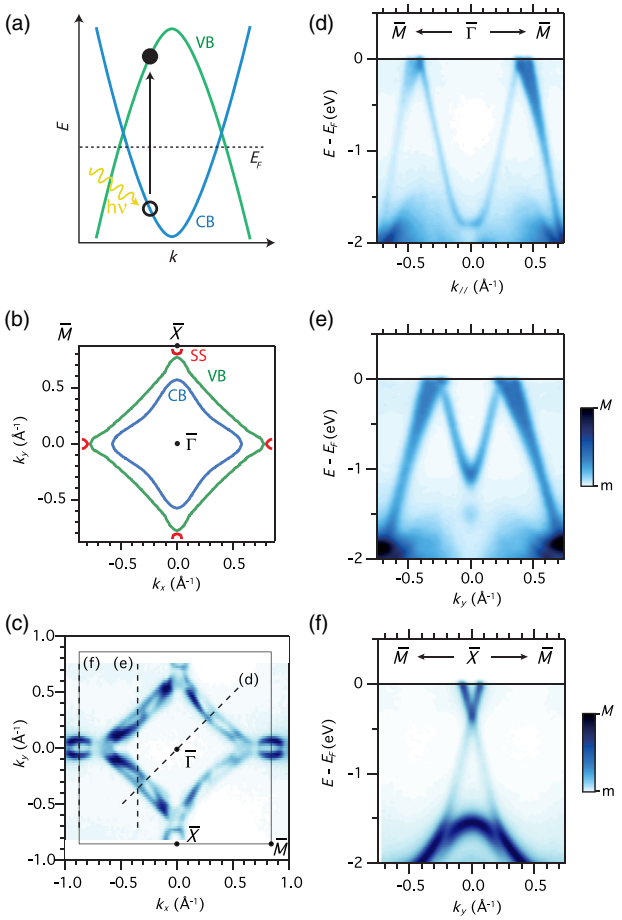


FIG. 1. (a) Sketch of the linearly dispersing Dirac states. Under intense laser light, electrons and holes are injected in the band structure far from the Dirac nodes, and can efficiently screen the Coulomb interaction. Calculated (b) and measured (c) Fermi surface of ZrSiSe. It consists of two diamond-shaped lines centered at $\bar{\Gamma}$, which originate from the valence band (VB, green) and the conduction band (CB, blue). An additional surface state (SS, red) is identified around $\bar{X}$, at the boundary of the surface Brillouin zone ($\bar{\Gamma}\bar{M} = 1.2$ Å$^{-1}$, $\bar{\Gamma}\bar{X} = 0.85$ Å$^{-1}$). (d)–(f) Experimental band dispersion, measured at 143 eV photon energy, along the black lines in panel (c). The two linearly dispersing bulk state, shown along the $\bar{\Gamma} - \bar{M}$ direction in (d), form the Dirac loop, with nodes above the Fermi level. Panels (e) and (f), shown as a reference for the TR-ARPES data in Fig. 2, illustrate the dispersion of the bulk (e) and surface (f) states near $E_F$.

The ARPES data of Fig. 1 provide a background for the TR-ARPES experiment. Figures 1(b) and 1(c) compare the theoretical and experimental Fermi surface, which consists

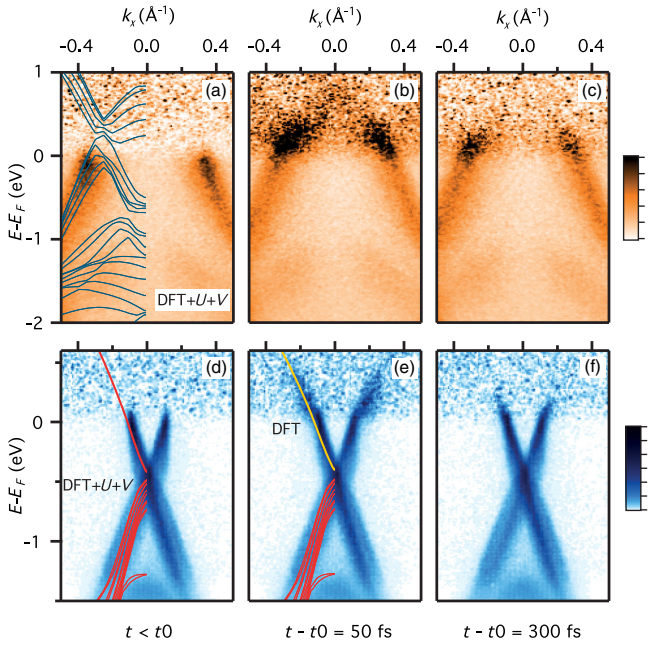


FIG. 2. (a)–(c) Band dispersion of the bulk bands, taken along the path (e) indicated in Fig. 1(c), for different delay times before (a), 50 fs after (b), and 300 fs after (c) the arrival of the optical excitation. Blue lines indicate the *ab initio* calculations for $U = 1.47$ eV and $V = 0.33$ eV. (d)–(f) Similar temporal evolution of the band structure along $\bar{M} - \bar{X} - \bar{M}$ [direction (f) in Fig. 1(c)], focusing on the dispersion of the surface state at different delay times. Red and yellow lines are the DFT + $U$ + $V$ and DFT calculations, respectively. In both the bulk and the surface states, a change in the band dispersion during optical excitation (50 fs) illustrates the light-induced renormalization of the band dispersion. The intensity at each binding energy is normalized to the same value integrated over the entire momentum window in order to increase the visibility of the signal above $E_F$.

of two diamond-shaped contours, corresponding to the CB (inner) and the VB (outer). A surface state (SS) forms short arcs around the $\bar{X}$ point of the surface Brillouin zone (SBZ) [red line in Fig. 1(b)] [28]. Dashed black lines in Fig. 1(c) indicate the cuts shown in Figs. 1(d)–1(f). Figure 1(d) displays the bands along the $\bar{\Gamma} - \bar{M}$ direction, where the VB and CB disperse linearly over a broad energy range, in good agreement with the literature [52]. Figures 1(e) and 1(f) show cuts parallel to the $\bar{M} - \bar{X} - \bar{M}$ direction, intercepting the bulk and the surface states, respectively.

Figure 2 illustrates the main result of our study. The TR-ARPES data measured at various delay times provide experimental evidence for the light-induced renormalization of the Dirac QP. Figure 2(a) shows the dispersion of the occupied bulk bands along the same direction as Fig. 1(e), for a photon energy of 36.9 eV. Due to the different matrix elements, the intensity of the inner CB state is strongly suppressed.

We find that standard DFT calculations cannot reproduce fine details of the band dispersion, in particular the precise binding energies of the valence and conduction bands. An on site $U = 5$ eV is needed in the DFT + $U$ calculations to correct the bands position. This unphysically large value cannot be reproduced by our self-consistent *ab initio* methods [39]. This highlights the partially delocalized character of electronic correlations in NLSMs, which are better accounted for by the intersite $V$ term. Our extended DFT + $U$ + $V$ Hubbard model predicts $U = 1.47$ eV and $V = 0.33$ eV, which are not free parameters but they are computed fully *ab initio*. The corresponding calculated band structure is shown in blue lines in Fig. 2(a), revealing excellent agreement with our data. A more detailed comparison between different computational methods is shown in the Supplemental Material [39]. A correlation phase diagram has been recently proposed, based on the reduction of spectral weight in the Drude peak [25]. ZrSiSe exhibits only moderate correlations, which produce small but noticeable changes in its electronic structure.

Figure 2(b) shows that 50 fs after optical excitation, electrons populate the bulk bands above $E_F$, and their dispersion seems to deviate from the theoretical predictions. The broadening of the bulk bands, which reflects their intrinsic $k_z$ dispersion, hampers a quantitative analysis of this effect. Therefore, we turn our attention to the sharper surface state, whose unperturbed dispersion is shown in Fig. 2(d) along the $\bar{M} - \bar{X} - \bar{M}$ direction. Red lines show the DFT + $U$ + $V$ calculations, which nicely reproduces not only the surface state dispersion but also the dispersion of the VB bands at lower energies. Upon optical excitation, in Fig. 2(e), electrons are excited well above $E_F$, and the band dispersion appears kinked. The band velocity is reduced with respect to the equilibrium one, and it is now better described by the simple DFT calculation shown as yellow lines. This effect will be analyzed quantitatively in Fig. 3. Here we notice that the timescale of the band renormalization is within the temporal resolution of our setup. Already 300 fs after the arrival of the pump pulse the band dispersion has recovered the equilibrium slope [Fig. 2(f)], only with the electronic system at a larger effective temperature. The ultrafast timescale suggests a purely electronic origin for the light-induced band renormalization, and it cannot be reconciled with the lattice motion. Moreover, the observed kink in the optically excited band structure cannot be ascribed to the coupling to a phonon, which would affect the dispersion in limited energy windows both above and below $E_F$ corresponding to the energy of the specific mode. By contrast, the observed change in dispersion extends well above the largest phonon energy (50 meV) in ZrSiSe [53,54].

Theory and experiment are quantitatively compared in Fig. 3. We simulate the ARPES intensity in Fig. 3(a) starting from the DFT + $U$ + $V$ calculation, broadened to account for the experimental resolution. The band occupancy is determined by the effective electronic temperature ($T^*$) estimated from a Fermi-Dirac fit to the experimental data

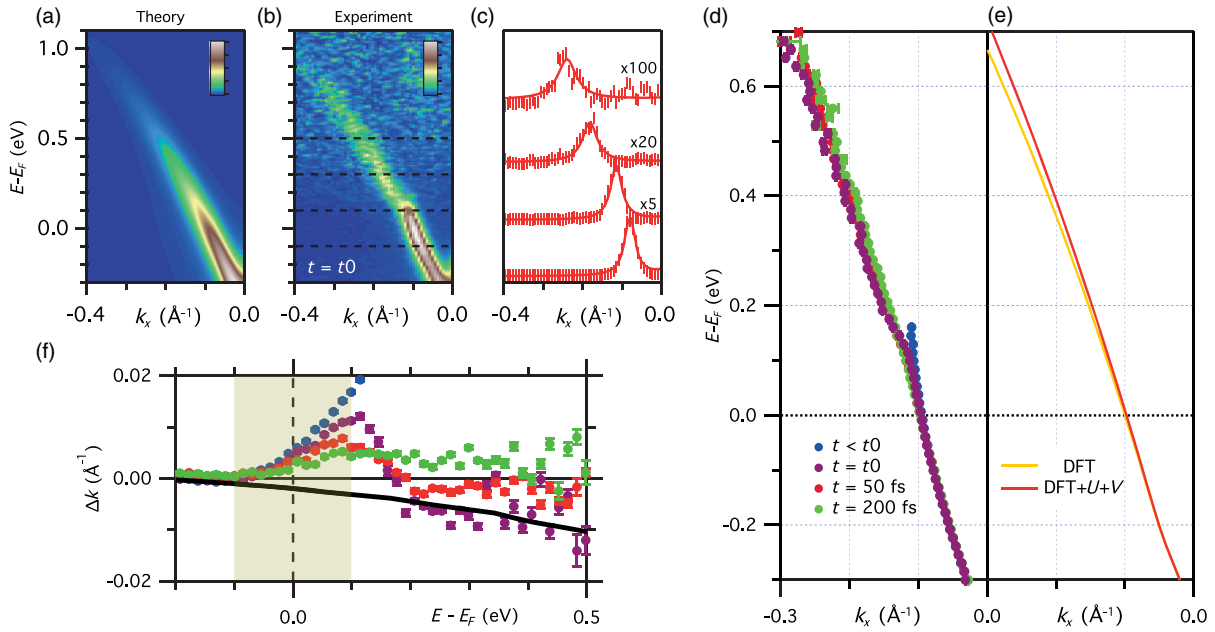


FIG. 3. (a) Simulated ARPES intensity from the *ab initio* calculations for $U = 1.47$ eV and $V = 0.33$ eV, broadened by the experimental momentum and energy resolution. The electron occupancy is defined by a Fermi-Dirac distribution for an effective temperature $T^* = 600$ K, as inferred from the experimental data at 200 fs. (b) Experimental spectral function at $t0$, during optical excitation. (c) MDCs at selected energies, indicated in (b) by dashed lines, and Lorentzian fits. (d) Peak positions as a function of energy; colors correspond to different delay times. (e) Calculated band dispersion for DFT + $U$ + $V$ (red) and DFT (yellow), respectively. (f) Change in band position, $\Delta k$, obtained as the difference between the experimental and peak position calculated with DFT + $U$ + $V$. The black line indicates the theoretical $\Delta k$ obtained as difference between the DFT and the DFT + $U$ + $V$ calculations.

200 fs after optical excitation ($T^* \approx 600$ K) [39]. The experimental dispersion is determined from Lorentzian fits to the momentum distribution curves (MDCs) extracted from the data, as shown in Fig. 3(c) for selected energies. The QP energies are shown in Fig. 3(d), where different colors encode the corresponding delay times during and immediately after optical excitation. The flattening of the band is well captured by the change in dispersion between the DFT + $U$ + $V$ (red) and DFT (yellow) calculated bands, as shown in Fig. 3(e). We plot in Fig. 3(f) the momentum renormalization $\Delta k$, i.e., the difference between the experimental (markers) and the dispersion calculated by DFT + $U$ + $V$. The difference between DFT and DFT + $U$ + $V$ dispersion is also plotted as reference (black line). For $E - E_F \geq 150$ meV $\Delta k$ is negative and as large as $-0.01 \pm 0.003$ Å$^{-1}$. The renormalization is largest during optical excitation (purple markers), and suddenly decreases after the pump pulse (red markers). The momentum renormalization $\Delta k$ is found to vary with the pump fluence, as discussed in the Supplemental Material [39]. We benchmark our interpretation by carrying out time-dependent DFT + $U$ + $V$ simulations of the TR-ARPES data. These additional results are discussed in the Supplemental Material [39], and they show that upon optical excitation the energy position of the states above $E_F$ corresponds to the one calculated by DFT, due to the transient screening of the electronic correlations. The band renormalization is a general effect, it affects the bulk states as well as the surface state, which is trivial and caused by a symmetry reduction at the surface [31].

Finally, we address the apparent kinklike structure observed in Fig. 3(b) and highlighted by the shaded area in Fig. 3(f). While the optical excitation tends to reduce the band velocity, an opposite contribution comes as a trivial consequence of the Fermi-Dirac function. As it is generally well established, at low temperature the sharp Fermi-Dirac cutoff strongly influences the intensity distribution around $E_F$, and the peak position estimated from the MDCs analysis deviates from the original band dispersion [55]. The evolution of this effect with the electronic temperature is discussed in details in the Supplemental Material, where we show that only at very high-electronic temperature the MDC analysis recovers the calculated band position near $E_F$ [39]. In our experimental result, the thermal effect is responsible for a positive $\Delta k$ at low temperature. Interestingly, this effect is visible at negative delay time, and it persists during the optical excitation, which indicates that electrons have not yet thermalized to high electronic temperatures. According to our analysis of the temporal dynamics of the Fermi-Dirac distribution [39], for the fluence used in the data set of Fig. 3, electrons fully thermalize via electron-electron scattering after 200 fs (green markers). Only when a hot thermalized electron distribution is established, do the broader Fermi

distribution cancel the positive $\Delta k$, and the band follows the DFT + $U$ + $V$ dispersion both around $E_F$ and at larger energies. This observation establishes a clear hierarchy between the timescales of the band renormalization and of electron-electron scattering and thermalization in ZrSiSe.

In summary, by combining time-resolved ARPES, *ab initio* DFT + $U$ + $V$ calculations and time-dependent DFT + $U$ + $V$ simulations we have shown that correlations can be optically modified in ZrSiSe, resulting in a QP renormalization. The equilibrium band structure is well reproduced by moderate on site $U = 1.47$ eV and an intersite $V = 0.33$ eV Coulomb terms, consistent with the reduced electronic screening of the Dirac QP. Upon optical excitation, the enhanced screening by high-energy electrons and holes produces a measurable change in the band dispersion. Previous TR-ARPES experiments have revealed ultrafast changes in the band dispersion of strongly correlated electron systems such as the high-temperature cuprate superconductors (HTSCs). They show changes of the coherent spectral weight [56], of the QP scattering rate [57] or of the QP effective mass [58]. These effects have been interpreted in terms of an optically induced reduction of the phase coherence, a mechanism which is specific to HTSC. Here we have shown that the QP dispersion can be controlled by purely electronic means, by changing the electronic screening of the Coulomb interaction. Our results are the first experimental evidence of a more general mechanism, originally proposed to control the electronic dispersion of correlated metal oxides [59], which we extend to the Dirac QP in NLSMs. Our findings demonstrate how ultrafast optical doping can be used as an alternative way of controlling quasiparticle properties, by tuning many-body interactions on a fs timescale. In particular, this could be exploited in other topological materials with linearly dispersing Dirac and Weyl states, where electronic correlations are believed to enhance the electron mobility [60] or to induce Lifshitz transitions [61].

We acknowledge financial support by the Swiss National Science Foundation (SNSF), via the NCCR:MUST and the Contracts No. 206021-157773 and No. 407040-154056 (PNR 70). This work was supported by the ERC Advanced Grant No. H2020, ERCEA Grant No. 695197, DYNAMOX Grant No. ERC-2015-AdG694097, the Cluster of Excellence (AIM), Grupos Consolidados (Grant No. IT1249-19), and SFB925. The Flatiron Institute is a division of the Simons Foundation. S. M. acknowledges support by the Swiss National Science Foundation (Grant No. P300P2-171221). This research used resources of the Advanced Light Source, which is a DOE Office of Science User Facility under Contract No. DE-AC02-05CH11231.

G. G. and A. C. equally contributed to this work.

*alberto.crepaldi@epfl.ch

[1] B. A. Bernevig, T. L. Hughes, and S.-C. Zhang, Science **314**, 1757 (2006).
[2] M. Z. Hasan and C. L. Kane, Rev. Mod. Phys. **82**, 3045 (2010).
[3] X. Wan, A. M. Turner, A. Vishwanath, and S. Y. Savrasov, Phys. Rev. B **83**, 205101 (2011).
[4] A. A. Burkov, M. D. Hook, and L. Balents, Phys. Rev. B **84**, 235126 (2011).
[5] S. M. Young, S. Zaheer, J. C. Y. Teo, C. L. Kane, E. J. Mele, and A. M. Rappe, Phys. Rev. Lett. **108**, 140405 (2012).
[6] N. P. Armitage, E. J. Mele, and A. Vishwanath, Rev. Mod. Phys. **90**, 015001 (2018).
[7] A. A. Burkov, J. Phys. Condens. Matter **27**, 113201 (2015).
[8] J. Gonzáles, F. Guinea, and M. A. H. Vozmediano, Phys. Rev. B **59**, R2474 (1999).
[9] T. Ando, J. Phys. Soc. Jpn. **75**, 074716 (2006).
[10] P. Hosur, S. A. Parameswaran, and A. Vishwanath, Phys. Rev. Lett. **108**, 046602 (2012).
[11] B. Roy, Phys. Rev. B **96**, 041113(R) (2017).
[12] Z. Wang and S.-C. Zhang, Phys. Rev. B **87**, 161107(R) (2013).
[13] B.-J. Yang, E.-G. Moon, H. Isobe, and N. Nagaosa, Nat. Phys. **10**, 774 (2014).
[14] Y. Huh, E.-G. Moon, and Y. B. Kim, Phys. Rev. B **93**, 035138 (2016).
[15] Y. Kim, B. J. Wieder, C. L. Kane, and A. M. Rappe, Phys. Rev. Lett. **115**, 036806 (2015).
[16] C. Fang, H. Weng, X. Dai, and Z. Fang, Chin. Phys. B **25**, 117106 (2016).
[17] S. V. Syzranov and B. Skinner, Phys. Rev. B **96**, 161105(R) (2017).
[18] S. Klemenz, S. Lei, and L. M. Schoop, Annu. Rev. Mater. Res. **49**, 185 (2019).
[19] J. Hu, Z. Tang, J. Liu, X. Liu, Y. Zhu, D. Graf, K. Myhro, S. Tran, C. N. Lau, J. Wei *et al.*, Phys. Rev. Lett. **117**, 016602 (2016).
[20] J. Hu, Z. Tang, J. Liu, Y. Zhu, J. Wei, and Z. Mao, Phys. Rev. B **96**, 045127 (2017).
[21] M. N. Ali, L. M. Schoop, C. Garg, J. M. Lippmann, E. Lara, B. Lotsch, and S. S. P. Parkin, Sci. Adv. **2**, e1601742 (2016).
[22] X. Wang, X. Pan, M. Gao, J. Yu, J. Jiang, J. Zhang, H. Zuo, M. Zhang, Z. Wei, W. Niu *et al.*, Adv. Electron. Mater. **2**, 1600228 (2016).
[23] R. Singha, A. K. Pariaria, B. Satpatia, and P. Mandala, Proc. Natl. Acad. Sci. U.S.A. **114**, 2468 (2017).
[24] S. Pezzini, M. R. van Delft, L. M. Schoop, B. V. Lotsch, A. Carrington, M. I. Katsnelson, N. E. Hussey, and S. Wiedmann, Nat. Phys. **14**, 178 (2017).
[25] Y. Shao, A. N. Rudenko, H. J, Z. Sun, Y. Zhu, S. Moon, A. J. Millis, S. Yuan, A. I. Lichtenstein, D. Smirnov *et al.*, Nat. Phys. **16**, 636 (2020).
[26] A. N. Rudenko, E. A. Stepanov, A. I. Lichtenstein, and M. I. Katsnelson, Phys. Rev. Lett. **120**, 216401 (2018).
[27] M. M. Scherer, C. Honerkamp, A. N. Rudenko, E. A. Stepanov, A. I. Lichtenstein, and M. I. Katsnelson, Phys. Rev. B **98**, 241112(R) (2018).

[28] L. M. Schoop, M. N. Ali, C. Strasser, A. Topp, A. Varykhalov, D. Marchenko, V. Duppel, S. S. Parkin, B. V. Lotsch, and C. R. Ast, Nat. Commun. **7**, 11696 (2016).
[29] M. Neupane, I. Belopolski, M. M. Hosen, D. S. Sanchez, R. Sankar, M. Szlawska, S.-Y. Xu, K. Dimitri, N. Dhakal, P. Maldonado *et al.*, Phys. Rev. B **93**, 201104(R) (2016).
[30] C. Chen, X. Xu, J. Jiang, S.-C. Wu, Y. P. Qi, L. X. Yang, M. X. Wang, Y. Sun, N. B. M. Schröter, H. F. Yang *et al.*, Phys. Rev. B **95**, 125126 (2017).
[31] A. Topp, R. Queiroz, A. Grüneis, L. Müchler, A. W. Rost, A. Varykhalov, D. Marchenko, M. Krivenkov, F. Rodolakis, J. L. McChesney *et al.*, Phys. Rev. X **7**, 041073 (2017).
[32] T. Nakamura, S. Souma, Z. Wang, K. Yamauchi, D. Takane, H. Oinuma, K. Nakayama, K. Horiba, H. Kumigashira, T. Oguchi *et al.*, Phys. Rev. B **99**, 245105 (2019).
[33] N. Tancogne-Dejean and A. Rubio, arXiv:1911.10813v1.
[34] A. Crepaldi, S. Roth, G. Gatti, C. A. Arrell, J. Ojeda, F. van Mourk, P. Bugnon, A. Magrez, H. Berger, M. Chergui *et al.*, Chimia **71**, 273 (2017).
[35] J. Ojeda, C. A. Arrell, J. Grilj, F. Frassetto, L. Mewes, H. Zhang, F. van Mourik, L. Poletto, and M. Chergui, Struct. Dyn. **3**, 023602 (2016).
[36] J. Ebad-Allah, J. F. Afonso, M. Krottenmüller, J. Hu, Y. L. Zhu, Z. Q. Mao, J. Kuneš, and C. A. Kuntscher, Phys. Rev. B **99**, 125154 (2019).
[37] M. B. Schilling, L. M. Schoop, B. V. Lotsch, M. Dressel, and A. V. Pronin, Phys. Rev. Lett. **119**, 187401 (2017).
[38] X. Andrade, D. Strubbe, U. De Giovannini, A. H. Larsen, M. J. T. Oliveira, J. Alberdi-Rodriguez, A. Varas, I. Theophilou, N. Helbig, M. J. Verstraete *et al.*, Phys. Chem. Chem. Phys. **17**, 31371 (2015).
[39] See the Supplemental Material at http://link.aps.org/supplemental/10.1103/PhysRevLett.125.076401 for more details about the analysis of the effective Fermi-Dirac distribution and the computational methods. It contains Refs. [38–48] (2019).
[40] C. P. Weber, B. S. Berggren, M. G. Masten, T. C. Ogloza, S. Deckoff-Jones, J. Madéo, M. K. L. Man, K. M. Dani, L. Zhao, G. Chen *et al.*, J. Appl. Phys. **122**, 223102 (2017).
[41] J. C. Johannsen, S. Ulstrup, F. Cilento, A. Crepaldi, M. Zacchigna, C. Cacho, I. C. Edmond Turcu, E. Springate, F. Fromm, C. Raidel, T. Seyller, F. Parmigiani, M. Grioni, and P. Hofmann, Phys. Rev. Lett. **111**, 027403 (2013).
[42] W. S. Fann, R. Storz, H. W. K. Tom, and J. Bokor, Phys. Rev. B **46**, 13592 (1992).
[43] G. Kresse and J. Hafner, Phys. Rev. B **47**, 558 (1993).
[44] P. E. Blöchl, Phys. Rev. B **50**, 17953 (1994).
[45] J. P. Perdew, K. Burke, and M. Ernzerhof, Phys. Rev. Lett. **77**, 3865 (1996).
[46] S. Grimme, J. Comput. Chem. **27**, 1787 (2006).
[47] J. Heyd, G. E. Scuseria, and M. Ernzerhof, J. Chem. Phys. **118**, 8207 (2003).
[48] Y. Klein, M. Casula, D. Santos-Cottin, A. Audouard, D. Vignolles, G. Fève, V. Freulon, B. Plaçais, M. Verseils, H. Yang, L. Paulatto, and A. Gauzzi, Phys. Rev. B **97**, 075140 (2018).
[49] L. A. Agapito, S. Curtarolo, and M. Buongiorno Nardelli, Phys. Rev. X **5**, 011006 (2015).
[50] N. Tancogne-Dejean, M. J. T. Oliveira, and A. Rubio, Phys. Rev. B **96**, 245133 (2017).
[51] U. De Giovannini, H. Hubener, and A. Rubio, J. Chem. Theory Comput. **13**, 265 (2017).
[52] M. M. Hosen, K. Dimitri, I. Belopolski, P. Maldonado, R. Sankar, N. Dhakal, G. Dhakal, T. Cole, P. M. Oppeneer, D. Kaczorowski, F. Chou, M. Z. Hasan, T. Durakiewicz, and M. Neupane, Phys. Rev. B **95**, 161101(R) (2017).
[53] W. Zhou, H. Gao, J. Zhang, R. Fang, H. Song, T. Hu, A. Stroppa, L. Li, X. Wang, S. Ruan *et al.*, Phys. Rev. B **96**, 064103 (2017).
[54] B. Salmankurt and S. Duman, Philos. Mag. **97**, 175 (2016).
[55] J. Gayone, C. Kirkegaard, J. Wells, S. Hoffmann, Z. Li, and P. Hofmann, Appl. Phys. A **80**, 943 (2005).
[56] C. L. Smallwood, J. P. Hinton, C. Jozwiak, W. Zhang, J. D. Koralek, H. Eisaki, D.-H. Lee, J. Orenstein, and A. Lanzara, Science **336**, 1137 (2012).
[57] F. Boschini, E. H. da Silva Neto, E. Razzoli, M. Zonno, S. Peli, R. P. Day, M. Michiardi, M. Schneider, B. Zwartsenberg, P. Nigge *et al.*, Nat. Mater. **17**, 416 (2018).
[58] J. D. Rameau, S. Freutel, L. Rettig, I. Avigo, M. Ligges, Y. Yoshida, H. Eisaki, J. Schneeloch, R. D. Zhong, Z. J. Xu *et al.*, Phys. Rev. B **89**, 115115 (2014).
[59] N. Tancogne-Dejean, M. A. Sentef, and A. Rubio, Phys. Rev. Lett. **121**, 097402 (2018).
[60] J. Fujioka, R. Yamada, M. Kawamura, S. Sakai, M. Hirayama, R. Arita, T. Okawa, D. Hashizume, M. Hoshino, and Y. Tokura, Nat. Commun. **10**, 362 (2019).
[61] N. Xu, Z. W. Wang, A. Magrez, P. Bugnon, H. Berger, C. E. Matt, V. N. Strocov, N. C. Plumb, M. Radovic, E. Pomjakushina *et al.*, Phys. Rev. Lett. **121**, 136401 (2018).